A practical fan-beam design and reconstruction algorithm for Active and Passive Computed Tomography of...

Article *in* Nuclear Instruments and Methods in Physics Research Section A Accelerators Spectrometers Detectors and Associated Equipment · May 2015

DOI: 10.1016/j.nima.2015.05.018

CITATION
1

READS
58

4 authors, including:

Tushar Roy
Bhabha Atomic Research Centre
23 PUBLICATIONS **47** CITATIONS
SEE PROFILE

Jilju Ratheesh
Bhabha Atomic Research Centre
3 PUBLICATIONS **3** CITATIONS
SEE PROFILE

Amar Kumar Sinha
Birat Medical college Teaching hospital, Nepal
73 PUBLICATIONS **492** CITATIONS
SEE PROFILE

Nuclear Instruments and Methods in Physics Research A 794 (2015) 164–170

Contents lists available at ScienceDirect

Nuclear Instruments and Methods in Physics Research A

journal homepage: www.elsevier.com/locate/nima

A practical fan-beam design and reconstruction algorithm for Active and Passive Computed Tomography of radioactive waste barrels

Tushar Roy*, M.R. More, Jilju Ratheesh, Amar Sinha

Neutron & X-Ray Physics Division, Bhabha Atomic Research Centre, Mumbai, India

ARTICLE INFO

Article history:
Received 28 February 2015
Received in revised form
11 May 2015
Accepted 11 May 2015
Available online 18 May 2015

Keywords:
Fan beam
Active and Passive CT
System matrix
MLEM

ABSTRACT

Active and Passive CT (A&PCT) of waste barrels is mostly carried out in parallel beam configuration due to its relative ease of implementation. This necessitates either using a single detector–source pair and translating the barrel or using multiple detector–source pairs for increasing the scanning speed. Additionally, because the use of bulky HPGe detectors may limit the number of detectors used in both active and passive modes, we propose to use $1'' \times 1''$ $LaBr_3(Ce)$ scintillators. This paper describes a practical fan-beam reconstruction for A&PCT imaging of waste barrels. A fan beam system model has been computed analytically and reconstruction done using MLEM algorithm. The results are compared with analytical reconstruction.

1. Introduction

Parallel beam reconstruction in Active and Passive CT (A&PCT) is widely used due to its rather simple set-up especially for large objects and scanning in three dimensions. A particular example is A&PCT of waste barrels [1–3]. In order to increase the scanning speed and waste drum throughput, multiple detectors (horizontal or vertical or both) in parallel beam configuration may be used and translation of the object or source–detector pair for scanning in-between positions. This yields a linear speedup by a factor approximately equal to the number of detectors used without a compromise in system accuracy. However, using multiple detectors in parallel beam configuration has a limitation in the Active CT step (Fig. 1(a)) since as many active sources (such as ^{152}Eu, ^{166m}Ho,^{60}Co) as the number of detectors are required. This is practically not easy due to the increase in cost as well as shielding required for multiple active sources. Another limitation is the use of HPGe detectors for waste assay. Since HPGe detectors are bulky and cannot be stacked vertically, it puts a limitation on the number of detectors that can be used (as the maximum horizontal span of the detectors should be equal to the width of the barrel).

One of the solutions is to use alternate detectors to HPGe. Roy et al. [4] have used $LaBr_3(Ce)$ detectors for SPECT imaging of simulated waste drums. A more practical approach is to devise new scanning geometries. Roberson et al. [5] have discussed some scanning configurations to this effect. One of the scanning methods is a fan-beam geometry with the active source placed at the focal point of the fan (Fig. 1(b)). In this scenario, there is a possibility of speedup due to the elimination of discrete translation positioning in the active (and/or passive) mode(s). Also, the fan-beam design has only one source and a very simple source collimator compared to the parallel case. A disadvantage of fan-beam geometry is that fan-beam detector collimators are somewhat more complicated in construction when compared to the parallel collimators.

Fan beam reconstruction has also been used by few other researchers [6–11] but has been mainly limited to proof-of-principle experiments or validation of new algorithms [8,9] or intended for small objects for clinical use [10]. There is very limited literature available on practical application of fan-beam reconstruction for large objects, such as waste drums. This paper describes a practical fan-beam reconstruction for A&PCT imaging of waste barrels. In the experimental design, the detectors are spaced equally along a straight line with collimators arranged in a fan beam configuration such that the collimator face is perpendicular to the line joining the focal point and detector center. A simplification introduced is in the use of flat fan-beam collimators instead of curved fan-beam collimators. For large objects and large focal length, the angular difference of a fan beam collimator and a parallel beam collimator is very small (for example, in the present experiment the angular difference is less than 4°). This makes the implementation of fan beam geometry easy and is a more practical solution.

Another aspect covered in the paper is the construction of fan beam system model. This paper describes an analytical computation of the fan beam system model and also its implementation for reconstruction using Maximum Likelihood – Expectation Maximization (MLEM) algorithm. The reconstruction results have been

* Corresponding author: Tel.: +91 22 25595492.
E-mail address: tushar@barc.gov.in (T. Roy).

http://dx.doi.org/10.1016/j.nima.2015.05.018
0168-9002/

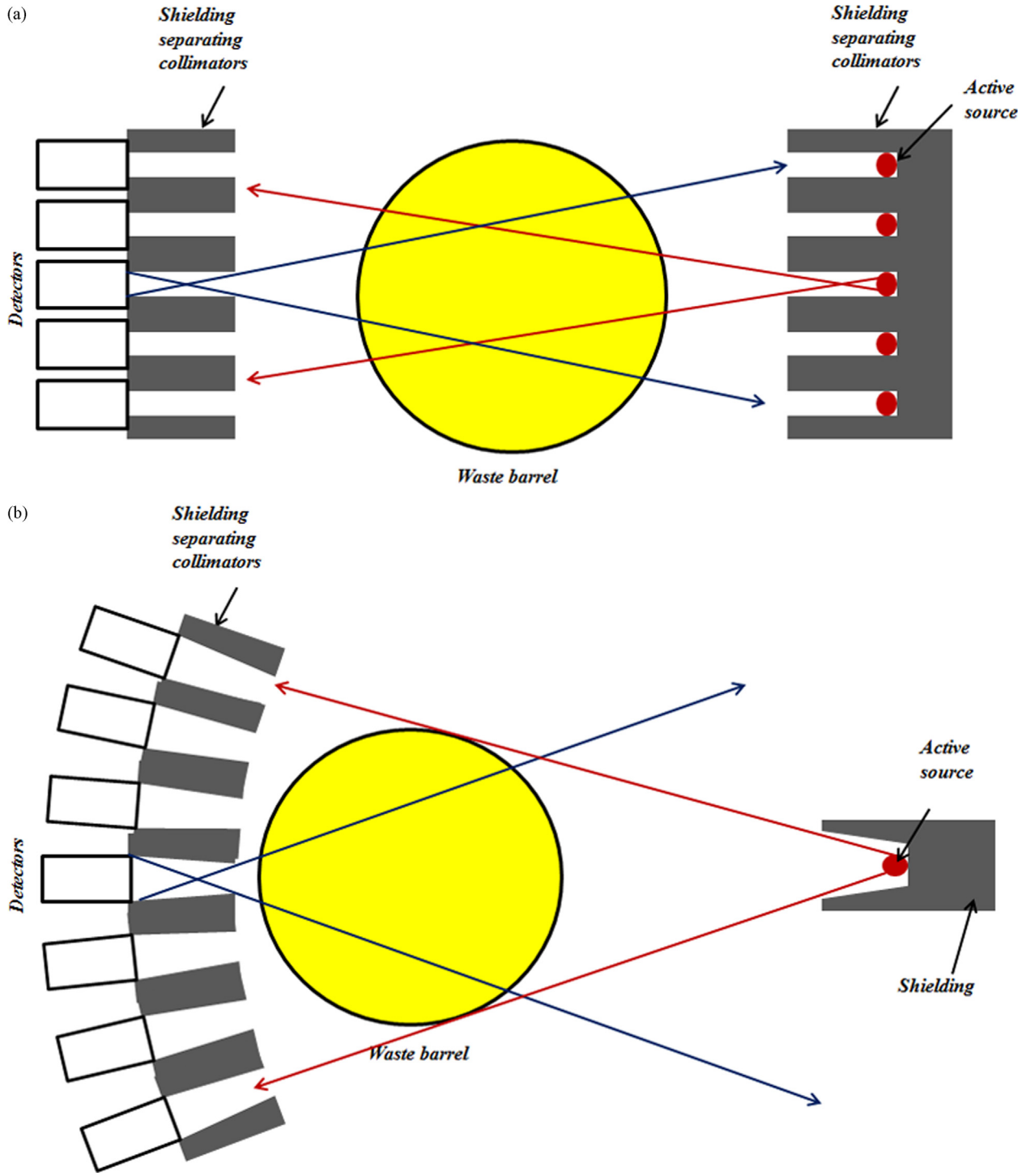

Fig. 1. Schematic arrangement for multiple detector A&PCT scan in (a) parallel beam and (b) fan beam configurations showing the requirement of active source(s).

compared with analytical fan beam reconstruction scheme proposed by You et al. [7].

2. Analytical fan-beam reconstruction with equally spaced detectors

You et al. [7] presented a modified FDK-like algorithm for extending Novikov's Inversion Formula [12] to fan beam reconstruction. We present a brief description of the formula.

Let S be the fan-beam focal point located at distance R from the origin. The projection data $\tilde{g}(\beta,u)$ measured at a position u on the detector at a view angle β (Fig. 2) is given by [7]:

$$\tilde{g}(\beta,u)=(\tilde{D}_{\mu}f)(\beta,u)=\int_0^{\infty} f(\underline{x}_s+t\underline{\alpha})e^{-(D\mu)(\underline{x}_s+t\underline{\alpha},\underline{\alpha})}dt \tag{1}$$

The inversion formula for the fan-beam geometry is given as [7]

$$f(\underline{x})=\frac{1}{4\pi}\mathrm{Re}\left\{\nabla\cdot\int_0^{2\pi}\frac{R^2}{U}\left\{\underline{\tilde{\beta}}\,e^{-\tilde{h}(\beta,u)+(D\mu)(\underline{x},-\underline{\beta}^{\perp})}\tilde{H}\frac{e^{\tilde{h}(\beta,u)}\tilde{g}(\beta,u)}{R^2+u^2}\right\}_{|\,u=u'}d\beta\right\} \tag{2}$$

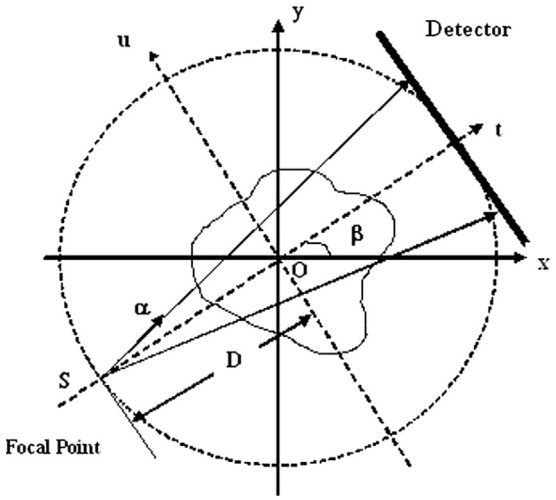

Fig. 2. Fan-beam geometry.

$$U=\frac{R+x\ \sin\ \beta-y\ \cos\ \beta}{R}$$

$$\underline{\tilde{\beta}}=\begin{pmatrix}\cos\left(\beta+\tan^{-1}\frac{u}{R}\right)\\ \sin\left(\beta+\tan^{-1}\frac{u}{R}\right)\end{pmatrix},$$

$$\tilde{h}(\beta,u)=\frac{1}{2}\left(I+i\tilde{H}\right)(\tilde{D}\mu)(\beta,u)=\frac{1}{2}\left(I+i\tilde{H}\right)\int_0^{\infty}\mu(\underline{x}_s+t\underline{\alpha})dt, \tag{3}$$

$\tilde{H}$ is the Hilbert transform defined in the fan-beam geometry [7]

$$u'=\frac{R(x\ \cos\ \beta+y\ \sin\ \beta)}{R+x\ \sin\ \beta-y\ \cos\ \beta}$$

3. Iterative fan-beam reconstruction with equally spaced detectors

For iterative reconstruction, we solve the system of equations

$$g=Af \tag{4}$$

where $g=(g_1,g_2,\ldots,g_M)^T$ is the observable (measured) data, i.e. projections, $f=(f_1,f_2,\ldots,f_N)^T$ is unknown spatial density distribution of nuclear disintegration events resulting in gamma emission in the object, and A is $M\times N$ system probability matrix (or projection matrix).

To solve Eq. (4), iterative techniques are used. In this paper, we have used a Maximum Likelihood – Expectation Maximization (MLEM) technique for reconstruction. It is one of the most common iterative algorithms used for SPECT reconstruction. In this formulation, a Poisson statistical model is applied to the projection data.

Mathematically, the MLEM formulation is stated as [13,14]

$$\hat{f}_j^{k+1}=\frac{\hat{f}_j^k}{\sum_{i=1}^{M}a_{ij}}\sum_{i=1}^{M}\frac{g_i}{\sum_{j'=1}^{N}a_{ij'}\hat{f}_{j'}^k}a_{ij} \tag{5}$$

As the correction factor in each iteration step is multiplicative in nature, non-negativity constraint is inherent in the MLEM technique.

Convergence criterion: To investigate the convergence properties of the implemented MLEM algorithm, following convergence criterion has been examined. The progress of the reconstruction is monitored by observing the root mean residual squares error (RMSE) at each iteration. RMSE is defined as follows:

$$\mathrm{RMSE}=\sqrt{\frac{1}{N}\sum_{i=1}^{N}(\hat{f}_i-f_i)^2} \tag{6}$$

$\hat{f}_i$ and f_i are the reconstructed and true activity value for *ith* pixel respectively and N is the total number of pixels. It is interpreted as how well the forward projection of the image matches with the measured data. Therefore it will be expected to decrease with increasing the iteration number, and approach to a plateau.

3.1. Computing the projection matrix

At the heart of any iterative technique is the computation of the system matrix. The accuracy of the techniques used in predicting f depends on how well the system matrix is modeled. In this section, we discuss an analytical method for computing the system matrix for fan beam reconstruction.

Neglecting scattering, we may write the system matrix as

$$A=A_{geom}\odot A_{att} \tag{7}$$

$\odot$ denotes element-by-element multiplication. To a first approximation, each element $A(i,j)$ can be expressed as

$$A(i,j)=\left[\frac{a_{ij}}{4\pi R_{ij}^2}\right]\left[\exp(-\sum_k\mu_k d_{ijk})\right]=A_{geom}(i,j)A_{att}(i,j) \tag{8}$$

a_{ij} is the area of the jth detector as seen by ith pixel,
R_{ij} is the distance between the ith pixel and jth detector,
μ_k is the attenuation coefficient of the kth pixel (material) lying on the ray path joining the ith pixel and jth detector,
d_{ijk} is the path length in kth pixel traversed by the gamma ray emitted from the ith pixel and reaching the jth detector.

3.1.1. Geometrical factor

The first term in Eq. (8) is the geometrical factor A_{geom}. The geometrical factor gives the contribution of the ith pixel at the jth detector due to geometrical conditions only. We shall consider the case with equally spaced detectors and parallel hole collimators. The detector–collimator pair is arranged such that the line joining the (virtual) focal point with detector (center) makes an angle η with x-axis, the collimator walls being parallel to this line. For 2D reconstruction, the object pixel and the detector are in the same plane. By simple geometrical consideration, the area of the jth detector as seen by ith pixel is given (from Fig. 3) as the difference of the projected width of w_c under angle β and the part of the projected width shadowed by the collimator.

$$a_{ij}=a-b=(w_c\ \cos(\beta-\eta)-l_c\ \sin(\beta-\eta))h_c \tag{9}$$

w_c is the collimator width,
l_c is the collimator length,
h_c is the collimator height,
β is the angle subtended by the ith pixel at the jth detector,
η is the fan angle of the jth detector.

From Fig. 3, if pixel and detector co-ordinates are (x_p,y_p) and (x_d,y_d) respectively, we can write

$$\cos\ \beta=\frac{x_d-x_p}{R_{ij}};\ \ \sin\ \beta=\frac{|y_d-y_p|}{R_{ij}} \tag{10}$$

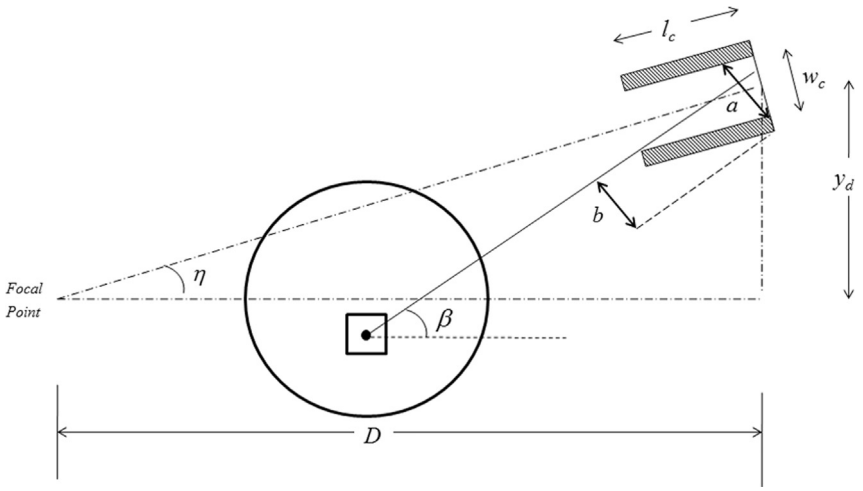

Fig. 3. Computing the geometrical factor of system matrix.

$$\cos\ \eta = \frac{D}{\sqrt{D^2+y_d^2}};\ \ \sin\ \eta = \frac{|y_d|}{\sqrt{D^2+y_d^2}} \tag{11}$$

The calculation of the geometrical factor depends on the shape of the holes in the collimator. For square hole collimator $h_c = w_c$. If collimator is further divided by septa into n holes per dimension, Eq. (9) is modified as

$$a_{ij} = (w_c\ \cos(\beta-\eta) - n.l_c\ \sin(\beta-\eta))h_c \tag{12}$$

Obviously, if $a_{ij} < 0$, the pixel does not contribute to the detector bin and we have to set $a_{ij} = 0$.

For other rotation angles, $A(i,j)$ is obtained by suitably rebinning the zero angle projection. This can be understood as follows. The zero-angle matrix is actually a matrix fixed to the coordinates of the collimator. When the object is rotated by an angle theta about the axis of rotation, the observation matrix thus formed can be related to the zero-angle observation matrix as follows.

The activity matrix, say f^{2D}, under a rotation by angle θ transforms to the rotated activity matrix f_θ^{2D}. Let f and f_θ represent the vectorized form of matrices f^{2D} and f_θ^{2D} respectively. We may then write

$$f_\theta = R_\theta f \tag{13}$$

where R_θ is a rotation matrix which relates the two vectors. Since we have rotated the image in the original co-ordinates, we can now write the geometrical factor of the system matrix for angle θ as

$$A_{\theta,geom} = A_{0,geom}R_\theta \tag{14}$$

We may write in matrix form as

$$A_{geom} = \begin{pmatrix} A_1 \\ A_2 \\ A_3 \\ \vdots \\ A_{n_\theta} \end{pmatrix} = \begin{pmatrix} A_0 I \\ A_0 R_2 \\ A_0 R_3 \\ \vdots \\ A_0 R_{n_\theta} \end{pmatrix} \tag{15}$$

where I is the identity matrix. The subscript *geom* has been dropped on the right side.

3.2. Attenuation factor

The second term in Eq. (8) is the attenuation factor A_{att}. The attenuation factor accounts for the net attenuation suffered by the gamma photon emitted from the ith pixel and reaching the jth detector. As stated in Eq. (8), the attenuation factor is given by

$$A_{att}(i,j) = \exp(-\sum_k \mu_k d_{ijk}) \tag{16}$$

The summation is done over all k pixels lying on the ray path joining ith pixel and jth detector. The procedure is then repeated for all $i = 1,2,\ldots,N_x.N_y$ and $j = 1,2,\ldots,N_y$.

Let $y(x)$ denote the line joining ith pixel and jth detector. Also, let $x = x_l$, $x = x_{l+1}$, $y = y_m$ and $y = y_{m+1}$ denote the left, right, bottom and top boundaries of kth pixel respectively. The line $y(x)$ can intersect k^{th} pixel in 6 ways as shown in Fig. 4 (ignoring the direction of the ray).

To find out the points of intersection, the following steps are followed:

- Find $y(x)|_{x=x_l}$ and $y(x)|_{x=x_{l+1}}$.
- If $y_m \le y(x)|_{x=x_l} \le y_{m+1}$, $y1 = y(x)|_{x=x_l}$ and $x1 = x_l$.
- If $y_m \le y(x)|_{x=x_{l+1}} \le y_{m+1}$, $y2 = y(x)|_{x=x_{l+1}}$ and $x2 = x_{l+1}$.
- If $y1 = null$ and $y2 \ne null$
  - If $y(x)|_{x=x_l} < y(x)|_{x=x_{l+1}}$, $y1 = y_m$, $x1 = y(x)|_{y=y_m}$.
  - If $y(x)|_{x=x_l} > y(x)|_{x=x_{l+1}}$, $y1 = y_{m+1}$, $x1 = y(x)|_{y=y_{m+1}}$.
- If $y1 \ne null$ and $y2 = null$
  - If $y(x)|_{x=x_l} < y(x)|_{x=x_{l+1}}$, $y2 = y_{m+1}$, $x2 = y(x)|_{y=y_{m+1}}$.
  - If $y(x)|_{x=x_l} > y(x)|_{x=x_{l+1}}$, $y2 = y_m$, $x2 = y(x)|_{y=y_m}$.
- $d_{ijk} = \sqrt{(x1-x2)^2+(y1-y2)^2}$.

In the above steps, $x1 = y(x)|_{y=y_m}$ means that $x1$ is equal to the value of x obtained by substituting $y = y_m$ in the equation $y(x) = 0$. If the line $y(x)$ does not intersect the kth pixel, d_{ijk} is set to zero.

However, the computation of the distances d_{ijk} for all projections would be computationally heavy task. Thus we use the same kind of method as in forming the geometrical factor. We first consider the zero angle projection and compute the distances d_{ijk} for all i,j,k. To compute the attenuation factor for other projections, we follow the same method as discussed above. The attenuation map vector after rotation may be written as

$$\mu_\theta = R_\theta \mu \tag{17}$$

where R_θ is the same rotation matrix as used above. The attenuation factor can now be written as

$$A_{\theta,att}(i,j) = \exp(-\sum_k \mu_{\theta,k} d_{ijk}) \tag{18}$$

The factors d_{ijk} obtained for the zero-angle projection are used.

Combining the geometrical and attenuation factors, the projection data at angle θ is now given by

$$g_\theta = (A_{\theta,geom} \odot A_{\theta,att})f = (A_{0,geom} \odot A_{\theta,att})R_\theta f \tag{19}$$

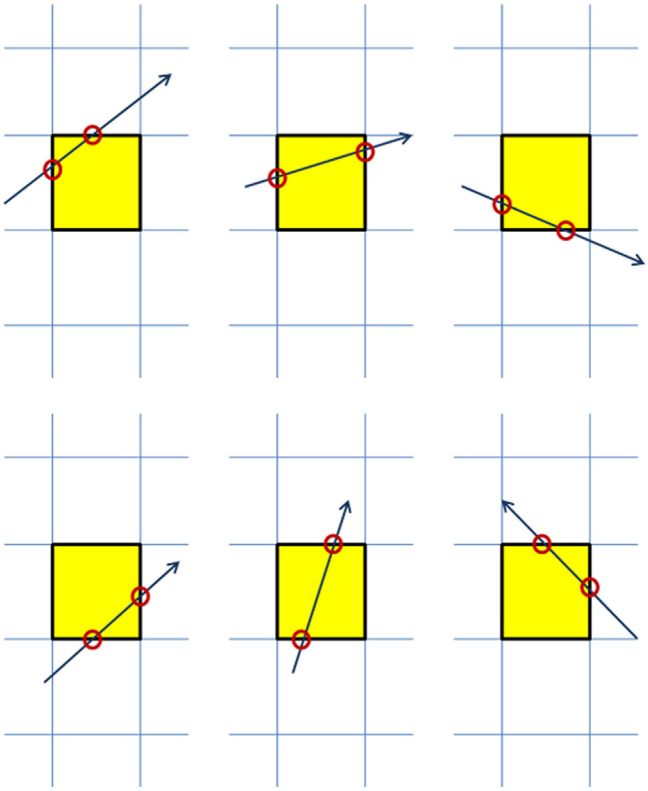

Fig. 4. Intersection of a ray with a pixel.

Hence, the complete system matrix can now be expressed as

$$A = \begin{pmatrix} (A_{0,geom} \odot A_{0,att})I \\ (A_{0,geom} \odot A_{2,att})R_2 \\ (A_{0,geom} \odot A_{3,att})R_3 \\ \vdots \\ (A_{0,geom} \odot A_{n_\theta,att})R_{n_\theta} \end{pmatrix} \tag{20}$$

where I is the identity matrix.

4. Experimental set-up

Fig. 5 shows a schematic of the experimental set up. It consists of the following:

a) *Sample stage*: Three axis (y, z, β) equip the mechanical support to move the waste drum. The drum is rotated and source–detector pair is elevated for complete scanning. For lateral scanning, the collimator–detector is manually arranged at desired positions.
b) *Detector*: $LaBr_3(Ce)$ detectors ($1'' \times 1''$) have been used.
c) *Collimator*: Parallel hole collimators have been used for the experiments. A lead collimator with tungsten septa has been used. The collimator opening of 25 mm is divided into 2×2 sections using tungsten septa (thickness 1.6 mm). The collimator length is 100 mm. The use of septa gives an effective collimation ratio of approximately 10:1 (for detailed description of the collimators, see [4]). The collimators have been arranged in a fan beam configuration, with the collimator face perpendicular to the line joining the virtual focal point and the detector (center). The detectors are equidistant spaced.
d) *Active source*: A 33 mCi ^{152}Eu source has been used for active scan. The physical dimension of the cylindrical source is approximately 3 mm (diameter) and 3 mm (height).

5. Experimental results

A mock-up waste barrel (580 mm diameter and 850 mm height) is filled with cotton waste/gloves/tissues/cellulose matrix. The apparent (global) attenuation coefficient of the matrix is .05 cm^{-1} (at 662 keV). Three ^{137}Cs sources have been placed at different locations inside the barrel. For Active CT measurement, a single external gamma source (^{152}Eu; 33 mCi) and three $LaBr_3(Ce)$

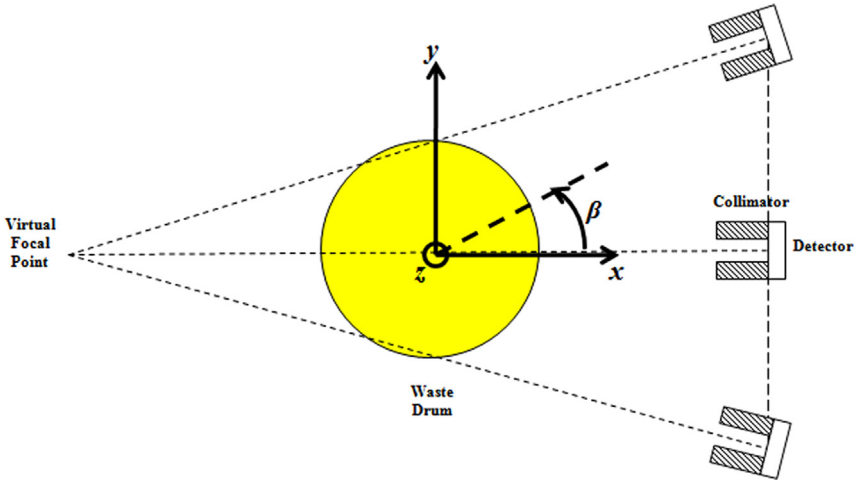

Fig. 5. Schematic of experimental set up.

detectors in an equally spaced fan beam configuration are used. Data has been acquired at 33 lateral positions and 15 angular positions over 180° for each z-position. In the vertical direction, 34 z-positions are scanned. Each slice thickness is 25 mm. The acquisition time for each scan is 5 s. The full-energy peak area corresponding to 121 keV, 244 keV, 344 keV, 444 keV, 778 keV and 964 keV is used for reconstructing the active data set. The attenuation coefficient at emission energy of 662 keV is obtained by interpolating the values pixel by pixel from the above data set. Fig. 6 shows the attenuation map at 662 keV obtained from the Active CT data. The attenuation map shows high density materials (densely packed rubber gloves) in the bottom one-third of the drum, nearly homogeneous attenuation in the middle one-third of the drum (nearly uniformly distributed cellulose matrix).

For passive CT, the detectors are used in the same configuration. Data is acquired at 33 lateral positions and 24 angular positions over 360° for each z-position. In the vertical direction, 34 z-positions are scanned. The focal length (distance of the focal point from the detector surface) is 1540 mm. The acquisition time for each data point is 10 s. The projection data are reconstructed on $33 \times 33 \times 34$ grid with reconstructed voxel size of 18 mm × 18 mm × 25 mm.

The projection data have been reconstructed using an analytical technique (Section 2, Eq. (2)) and MLEM reconstruction using the system model as discussed in Section 3. The number of iterations required for the MLEM technique is 50. Fig. 7(a) shows the analytical reconstruction for ^{137}Cs activity in the waste barrel. Fig. 7(b) shows the MLEM reconstruction using the system model as discussed in Section 3.

Fig. 8 shows the ^{137}Cs activity using analytical reconstruction (no collimator modeling) (top row) and MLEM reconstruction (bottom row) using the fan beam system model. The activity map for three consecutive z-slices is shown. It can be seen that the collimator blurring in the reconstruction plane is reduced in the MLEM reconstruction as the collimator modeling has been implemented in the system matrix. The MLEM reconstruction using the fan-beam projection-matrix gives a better spatial resolution than the analytical reconstruction. Table 1 shows the reconstructed activity and 1σ error for the three sources.

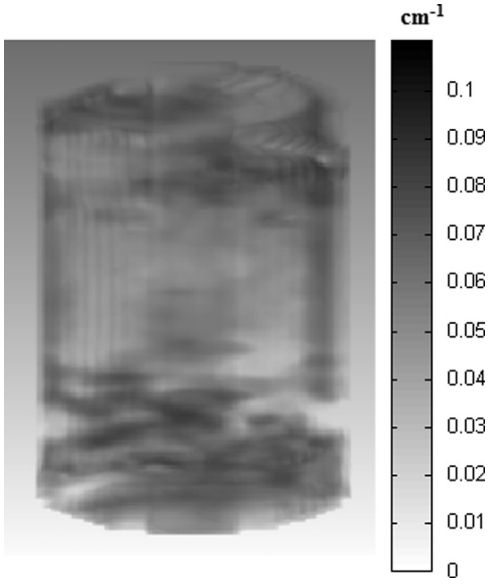

Fig. 6. Reconstructed attenuation map at 662 keV.

6. Conclusion

An analytical method for computing projection-matrix for fan beam geometry with equally spaced detectors for SPECT imaging has been discussed in this paper. The system matrix has been used to reconstruct activity distribution in a mock-up waste barrel using MLEM algorithm. The quantitative results show that the MLEM reconstruction shows closer agreement with real ^{137}Cs activity of the source as compared to the analytical reconstruction. Also, MLEM reconstruction using the fan-beam projection-matrix gives a better spatial resolution than the analytical reconstruction. The fan-beam geometry discussed in the paper and its practical implementation offers the choice of using multiple detectors in active (and passive) mode(s) using a single active source, thus reducing the overall scanning time of the active mode by a factor approximately equal to the number of detectors used.

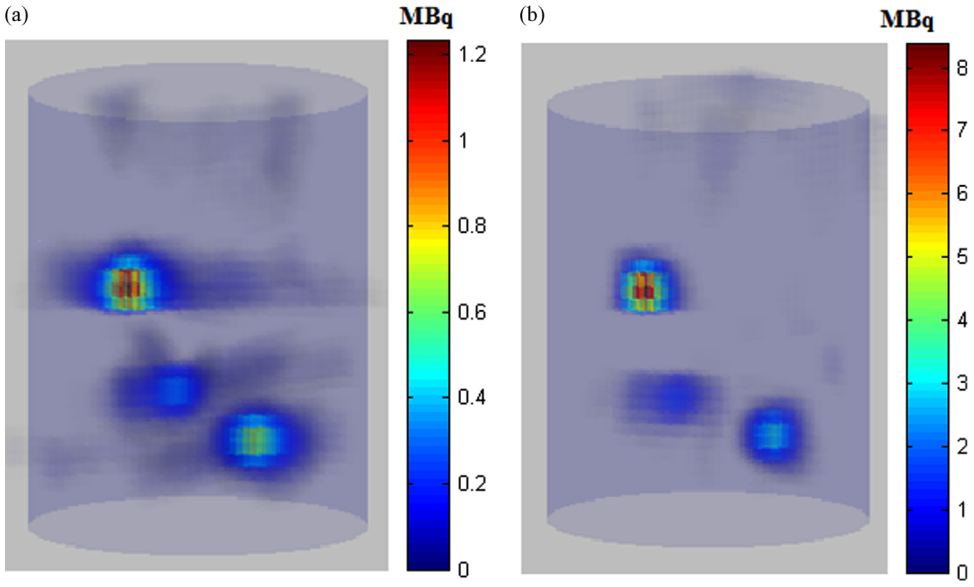

Fig. 7. (a) Analytical (b) MLEM reconstructed ^{137}Cs activity respectively (the drum outline is shown for illustration).

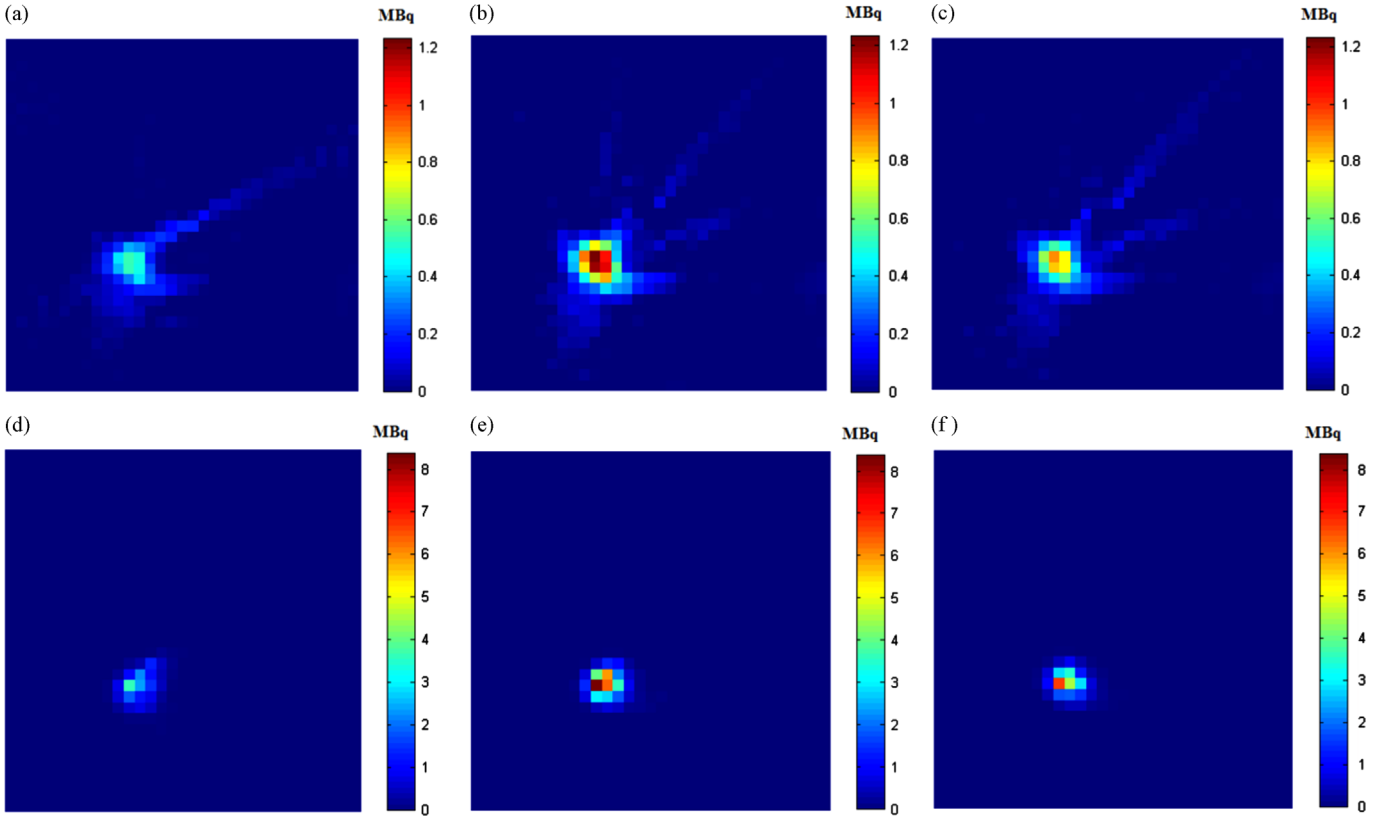

Fig. 8. ^{137}Cs activity for Slice 18, Slice 19 and Slice 20 (left to right) using analytical (a–c) and MLEM (d–f) reconstruction.

Table 1
Comparison of reconstructed and true source activity.

Source (Slice-wise location)	True activity (MBq)	Analytical		MLEM	
		Reconstructed activity (MBq)	Deviation from true activity (%)	Reconstructed activity (MBq)	Deviation from true activity (%)
A (Bottom)	26.7	24.9 ± 1.8	6.7	26.6 ± 1.6	.4
B (Middle)	21.0	18.7 ± 1.5	10.9	19.9 ± 1.4	5.2
C (Top)	37.8	35.1 ± 1.9	7.1	36.9 ± 1.8	2.4

References

[1] D.C. Camp, H.E. Martz, G.P. Roberson, D.J. Decman, R.T. Bernardi, Nondestructive waste-drum assay for transuranic content by gamma-ray active and passive computed tomography, Nuclear Instruments and Methods in Physics Research Section A 495 (2002) 69–83.

[2] G.P. Roberson, H.E. Martz, D.J. Decman, J.A. Jackson, D. Clark, R.T. Bernardi, D.C. Camp, Active and passive computed tomography for nondestructive assay, in: Proceedings of the Sixth Nondestructive Assay and Nondestructive Examination Waste Characterization Conference, Salt Lake City, Utah, November 17–19 (1998) 359.

[3] S. Croft, R. Venkataraman, M. Villani, R.J. Estep, On the accuracy of the tomographic gamma scanner for the assay of drummed waste, in: Proceedings of the Waste Management Conference (2004).

[4] Tushar Roy, Jilju Ratheesh, A. Sinha, Three-dimensional SPECT imaging with LaBr3:Ce scintillator for characterization of nuclear waste, Nuclear Instruments and Methods in Physics Research Section A 735 (2013) 1–6.

[5] G.P. Roberson, H.E. Martz, D.C. Camp, D.J. Decman, E.M. Johansson, Preliminary A&PCT Multiple Detector Design, Lawrence Livermore National Laboratory, USA, 1997 UCRL-ID-128052.

[6] Hongwei Ye, Development and Implementation of Fully 3D Iterative Reconstruction Approaches in SPECT with Parallel-, Fan- and Cone-Beam Collimators Ph.D. thesis, Syracuse University, 2008.

[7] J. You, G.L. Zeng, Z. Liang, FBP algorithms for attenuated fan-beam projections, Inverse Problems 21 (2005) 1179–1192.

[8] Q. Tang, G.L. Zeng, G.T. Gullberg, Analytical fan-beam and cone-beam reconstruction algorithms with uniform attenuation correction for SPECT, Physics in Medicine & Biology 50 (2005) 3153–3170.

[9] Q. Huang, G.L. Zeng, J. You, G.T. Gullberg, An FDK-like cone-beam SPECT reconstruction algorithm for non-uniform attenuated projections acquired using a circular trajectory, Physics in Medicine & Biology 50 (2005) 2329–2339.

[10] M.V. Narayanan, M.A. King, and C.L. Byrne, Combined Fan/Parallel Beam Reconstruction in Cardiac SPECT Imaging, in: Proc. Conf. Record IEEE NSS (1999).

[11] C. Miao, Comparative studies of different system models for iterative CT image reconstruction, Thesis of Wake Forest University (2013).

[12] R. Novikov, An inversion formula for the attenuated X-ray transformation, Arkiv för Matematik 40 (2002) 145–167.

[13] L.A. Shepp, Y. Vardi, Maximum likelihood reconstruction for emission tomography, IEEE Transactions on Medical Imaging 1 (2) (1982) 113–122.

[14] K. Lange, R. Carson, EM reconstruction algorithms for emission and transmission tomography, Journal of Computer Assisted Tomography 8 (2) (1984) 306–316.